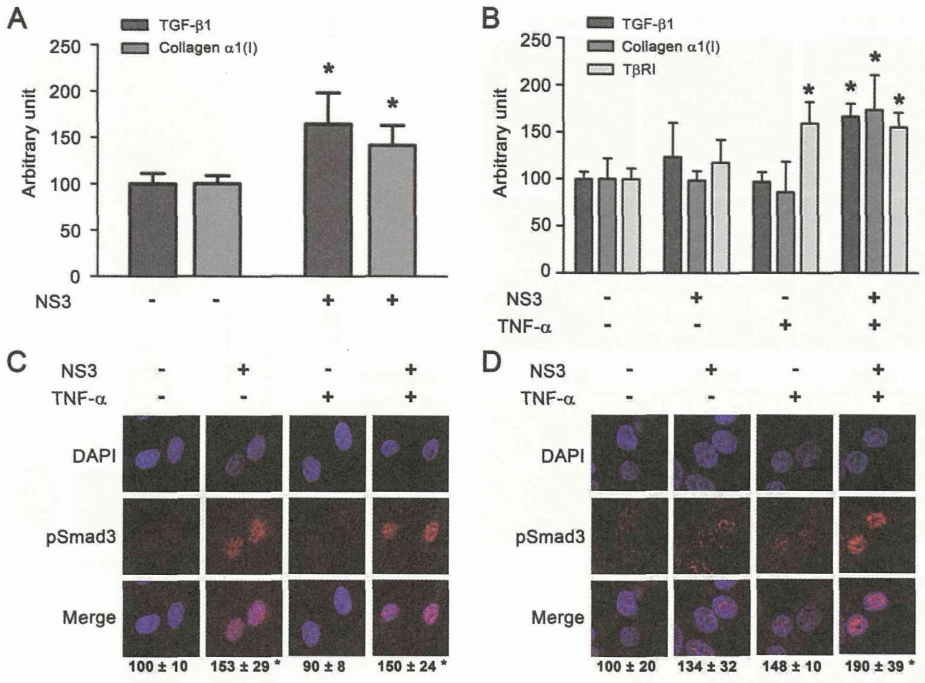

Figure 2 | Cooperativity between NS3 and TNF-α in the stimulation of TGF-β1, collagen α1(I), and TβRI expression. (A) Effect on TGF-β1 and collagen α1(I) mRNA expression in LX-2 cells. The cells were stimulated with 50 μg/ml of NS3 for 12 hours. Total cellular RNA was isolated and reverse transcribed to cDNA, and real-time PCR was performed as described in the Methods section. $*p < 0.05$ compared with untreated control cells. (B) Effect of pretreatment with TNF-α on the stimulation of expression of TGF-β1, collagen α1(I), and TβRI by NS3 protease in HC cells. Following the pretreatment of the cells with 20 ng/ml TNF-α for 12 hours, they were stimulated with 25 μg/ml NS3 for 12 hours, and mRNA expression was measured as described above. $*p < 0.05$ compared with untreated cells. The data are shown as the mean ± SD (n = 3). (C and D) The effect of pretreatment with TNF-α on the stimulation of phosphorylation of Smad3 by NS3 protease in LX-2 cells (C) and Hc cells (D). After the cells were treated with 20 ng/ml TNF-α for 12 hours and 25 μg/ml NS3 for another 12 hours, they were fixed, and immunofluorescent staining was performed as described in the Methods section. The experiments were performed in duplicate. The relative fluorescence intensities of phospho-Smad3 (% of untreated control cells) in 4 randomly selected fields from each dish were calculated with ZEN software and are shown as the mean ± SD. The results are representative of three independent experiments with similar results.

TβRI in the immunoprecipitation experiment (Supplementary Fig. S7A). Antibodies produced to these predicted binding sites within both NS3 and TβRI decreased the TGF-β mimetic activity of NS3 in $(CAGA)_9$-Luc CCL64 cells (Fig. 3F–H). Furthermore, the anti-NS3 antibody inhibited HCV-induced Smad3 phosphorylation (Supplementary Fig. S7B).

Anti-NS3 antibody prevented liver fibrosis in HCV-infected chimeric mice. To test our hypothesis that NS3 exerts TGF-β mimetic activity, thereby causing liver fibrosis, we examined whether the anti-NS3 antibody could prevent liver fibrosis in HCV-infected human hepatocyte-transplanted chimeric mice. The anti-NS3 antibody significantly prevented hepatic collagen accumulation in the mice (Fig. 4A) and decreased the mRNA expression of both TGF-β1 and collagen α1 (I) (Fig. 4B and 4C). There was no significant change in the serum levels of human albumin and HCV RNA during treatment with the anti-NS3 antibody (Supplementary Fig. S8A and S8B).

Discussion

Several groups have studied the molecular mechanisms by which HCV induces liver fibrosis and have reported the following: (i) HCV core protein activates the TGF-β1 promoter via the MAPK pathway in core protein-expressing human hepatocellular carcinoma HepG2 cells[11]; (ii) recombinant core protein upregulates the expression of fibrogenic genes in the human hepatic stellate cell line LX-2 via the toll-like receptor 2 [12] and the obese receptor[13]; and (iii) NS3 protease induces TGF-β1 production in NS3-over-expressing human hepatoma Huh-7 cells[14]. Our data show that NS3 protease mimics TGF-β2 and directly exerts its activity, at least in part, via binding to and activating TβRI, thereby enhancing liver fibrosis. The following experiments should be carried out in the future: effect of NS3 on TβRI phosphorylation, the expression of TGF-β2, TGF-β3, and other TGF-β responsive genes, such as plasminogen activator inhibitor-1, a tissue inhibitor of metalloproteinase-1, and α-smooth muscle actin, to further validate the TGF-β mimetic activity of NS3.

HCV NS3 is a chimera of a helicase and serine protease, which cleaves not only the junction between NS3-4A, NS4A-4B, NS4B-5A, and NS5A-5B for viral polyprotein processing, which is essential to the viral lifecycle, but also the toll-interleukin-1 receptor domain-containing, adaptor-inducing beta interferon, and mitochondrial antiviral signaling protein, which results in the disruption of innate immune responses[7,15]. An NS3 protease inhibitor, telaprevir, which was approved by the FDA in 2011, has been used in triple combination therapy with the current standard treatment of PEGylated interferon and ribavirin[16]. Telaprevir did not inhibit TGF-β mimetic activity in a $(CAGA)_9$-Luc reporter gene assay (Fig. 1C), suggesting that the TGF-β mimetic activity of NS3 is independent of its protease activity.

Much interest has centered on the fact that extraordinarily high concentrations of NS3 protease, up to 100 μg/ml, could exist in

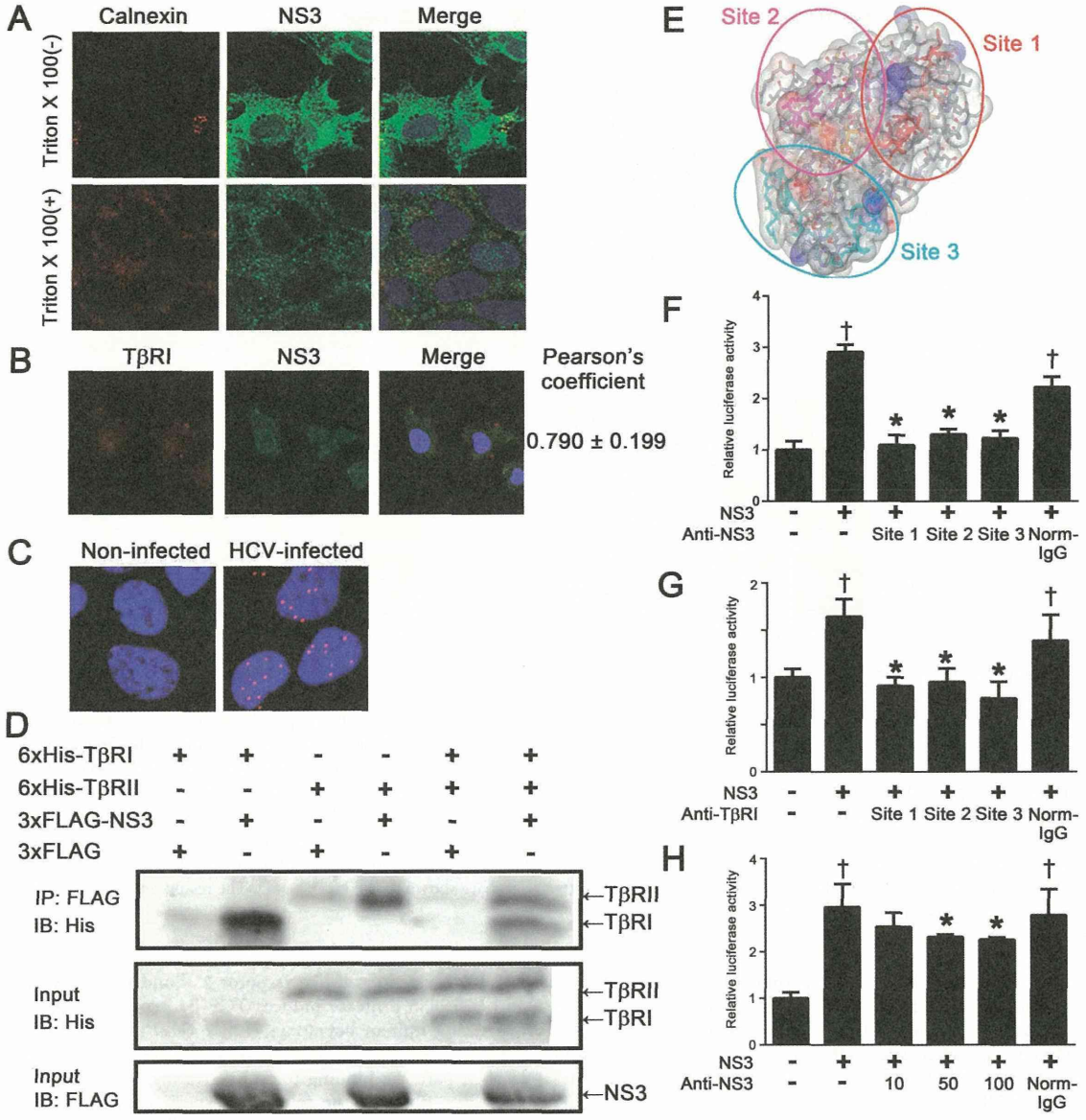

Figure 3 | NS3 protease colocalized and directly interacted with TβRI on the surface of HCV-infected cells. (A) The detection of NS3 protease on the surface of HCV-infected Huh-7.5.1 cells. The cells were fixed, followed ± by permeabilization with Triton-X 100, and then stained with DAPI, anti-NS3 antibody, and anti-calnexin antibody. (B) The colocalization of NS3 protease with TβRI in HCV-infected Huh7.5.1 cells. The cells were fixed and stained with DAPI, anti-NS3 antibody, and anti-TβRI antibody, as described in the Methods section. Pearson's colocalization coefficient values were obtained from 4 randomly selected fields using the ZEN software. The results are shown as the mean ± SD and are representative of three independent experiments with similar results. (C) The detection of NS3-TβRI proximity by in situ PLA in HCV-infected Huh-7.5.1 cells. The red dots indicate interactions between NS3 protease and TβRI, and the nuclei were identified by DAPI staining. (D) The physical interaction of NS3protease with TβRI and TβRII. FLAG-tagged NS3protease was incubated with 6xHis-tagged TβRI and/or TβRII and immunoprecipitated. The coprecipitated proteins were visualized by immunoblotting using anti-His antibody. The gels were run under the same experimental conditions. Cropped blots are shown (full-length blots are presented in Supplementary Fig. S5). (E) The structural overview of the NS3protease. The indicated colored amino acids (site 1, red; site 2, magenta; and site 3, cyan) show the important residues within the putative binding sites to TβRI, and the sequences are presented in Table 1. TGF-β mimetic activity of NS3 was inhibited in the presence of either anti-NS3 polyclonal antibodies against the predicted binding sites of TβRI (F), or anti-TβRI polyclonal antibodies against predicted binding sites of NS3 (G), and anti-NS3 monoclonal antibody against predicted binding site 3 of TβRI (H). Luciferase activities in $(CAGA)_9$-Luc CCL64 cells were measured as before. Normal mouse IgG (Norm-IgG) was used as a negative control. The data are shown as the mean ± SD. †$p < 0.05$ compared with untreated control cells, *$p < 0.05$ compared with NS3-treated cells without any antibodies. Representative results from three independent experiments with similar results are shown.

Table 1 | The amino acid sequences of predicted binding sites between NS3 protease and TβRI

	NS3 protease	TβRI
Site 1	TGRDKNQVEGEVQVVSTATQS	FVSVTETTDKVIHNSM
Site 2	TNVDQDLVGWPAPPGARSLTP	IAEIDLIPRDRPFV
Site 3	GDNRGSLLSPRPVSYLKGSS	CAPSSKTGSVTTTY

The underlined letters denote the putative contact residues.

proximity to a TGF-β receptor. This line of inquiry led us to identify the cooperativity between NS3 and TNF-α, although the cooperative effect was maximal at one fourth this concentration of NS3. Serum levels of TNF-α in chronic hepatitis C patients are known to be significantly higher than those in healthy subjects[17,18]. We showed that TNF-α increased the susceptibility of cells to NS3 by enhancing the expression of TβRI, thereby further increasing the levels of profibrogenic genes (Fig. 2B). Various hepatic cell lines expressed different levels of TβRI, and there appeared to be a threshold in the level of TβRI that enabled cells to produce collagen mRNA upon stimulation with NS3. In particular, Hc cells expressed levels of TβRI below this predicted threshold (Supplementary Fig. S9). Consistent with our findings, carbon tetrachloride has recently been reported to induce acute liver injury, specifically significant liver fibrosis with inflammation, in transgenic mice expressing the full-length HCV polyprotein[19].

We documented the colocalization of NS3 and TβRI on the cell surface of HCV JFH-1-infected Huh-7.5.1 cells (Fig. 3). The results of co-immunoprecipitation and in situ PLA studies supported this conclusion. In future studies, we intend to use mutagenesis experiments of the predicted binding site and competition assays using NS3 and TGF-β in $(CAGA)_9$-Luc CCL64 cells to determine the mechanism of NS3 and TβRI binding. However, at present, how NS3 is released to the extracellular milieu remains to be elucidated. One possibility is that NS3 leaks passively from injured hepatocytes, as is the case for alanine aminotransferase and aspartate aminotransferase. Another possibility is that NS3 is secreted from HCV-infected cells via the Golgi complex. A recent report showed that nonstructural protein (NS) 1 of the dengue virus (DENV) and West Nile virus (WNV) is secreted from DENV- and WNV-infected cells through the Golgi complex following expression in association with the endoplasmic reticulum. Like HCV, these viruses are also members of the family *Flaviviridae*[20].

Zhang et al.[21] identified antibodies against NS3 in the serum of chronic hepatitis C patients and suggested that extracellular NS3 may be present in such cases. However, it remains unclear whether the concentration of HCV NS3 is as high as in our in vitro experiments. Although DENV NS1 has been reportedly detected at high levels (up to 50 μg/ml) in the serum of DENV-infected patients[22], further study is warranted to determine the serum or tissue NS3 concentrations in patients with chronic hepatitis C.

In this study, we generated polyclonal and monoclonal anti-NS3 antibodies that block the NS3-TβRI interaction. All anti-NS3 and anti-TβRI polyclonal antibodies generated against the predicted binding sites almost completely blocked TGF-β mimetic activity. This finding was likely due to steric hindrance by these antibodies or a requirement of binding at all three sites for signal transduction by NS3. The monoclonal antibody is a powerful tool that can be used to explore our working hypothesis that NS3 enhances liver fibrosis via the TGF-β receptor *in vivo*. We showed that the anti-NS3 monoclonal antibody generated against a predicted binding site to TβRI ameliorated liver fibrosis in HCV-infected human hepatocyte transplanted chimeric mice (Fig. 4A–C). The control of fibrosis after the eradication of the virus determines the prognosis, including the likelihood of progression to tumorigenesis. Therefore, the NS3 antibody

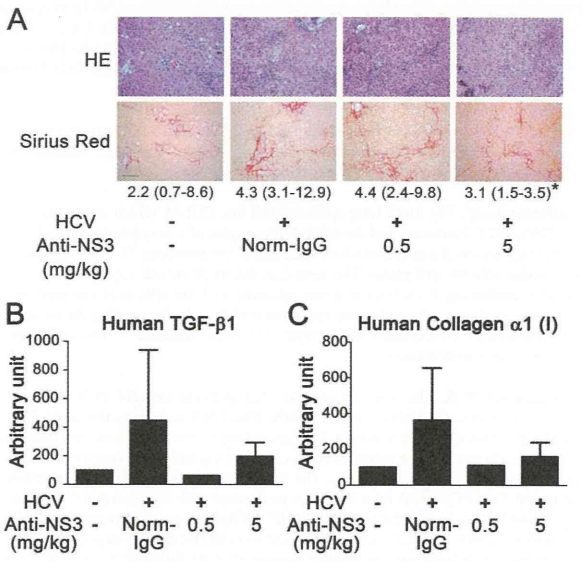

Figure 4 | Anti-NS3 antibody attenuated liver fibrosis in the HCV-infected chimeric mice. (A) Staining of liver sections. Paraffin sections were prepared from the livers of HCV-infected chimeric mice 16 weeks after HCV inoculation, and stained with hematoxylin and eosin (upper panels) and Sirius Red (lower panels). An anti-NS3 antibody was administered at the indicated doses, and normal mouse IgG (Norm-IgG) was administered at a dose of 5 mg/kg. For each group, the median ratios in Sirius Red positive/total area (%) from 6 randomly selected fields are shown, with the range in parentheses. $^*p < 0.05$ compared with HCV-infected mice without anti-NS3 antibody. Scale bar = 100 μm. The representative result from 6 randomly selected fields is shown. (B) and (C) Hepatic mRNA expression in HCV-infected chimeric mice. Total RNA was isolated from the livers of these mice and reverse transcribed to cDNA, and real-time PCR was performed as described in the Methods section to quantitate the expression of human TGF-β1 expression (B) and human collagen α1 (I) (C). The data are shown as the mean ± SD, and representative results from two independent experiments with similar results are shown.

against the TβRI binding site might have a clinical benefit in HCV patients with cirrhosis after combination therapy.

In conclusion, we demonstrated for the first time that HCV NS3 protease serves as a novel TGF-β receptor ligand and enhances liver fibrosis. This phenomenon might be beneficial to the virus, as TGF-β signals suppress host immunity. Our results provide elucidation regarding the molecular mechanism by which HCV induces liver fibrosis.

Methods

Materials. SB-431542 and LY-364947 were purchased from Sigma-Aldrich (St. Louis, MO). Recombinant human TNF-α was purchased from R&D systems, Inc. (Minneapolis, MN). Anti-NS3 antibody and anti-calnexin antibody were purchased from Abcam (Cambridge, UK). Anti-TβRI antibody and anti-phospho-Smad3 antibody were purchased from Santa Cruz Biotechnology (Santa Cruz, CA) and Immuno-Biological Laboratories (Gunma, Japan), respectively. Anti-Flag M2 antibody and anti-His antibody were purchased from Sigma (St. Louis, MO). Anti-NS3 antibodies and anti-TβRI antibodies against predicted binding sites were provided by the BioMatrix Research Institute (Chiba, Japan).

Cell culture. $(CAGA)_9$-Luc CCL64 cells were kindly provided by Prof. Hideaki Kakeya (Kyoto University, Kyoto, Japan), the hepatic stellate cell line LX-2 was kindly provided by Prof. Norifumi Kawada (Osaka City University, Osaka, Japan), and the human hepatoma cell line Huh-7.5.1 were maintained in Dulbecco's modified Eagle's medium (DMEM) supplemented with 10% fetal bovine serum, penicillin, and streptomycin. HC cells, a normal human hepatocyte cell line purchased from Cell Systems (Kirkland, WA), were cultured in CS-C complete medium (Kirkland, WA).

Protein preparation. The N-terminal histidine or 3xFLAG-tagged NS3 protease, and the extracellular domain of human TβRI and TβRII were expressed in *Escherichia coli* by isopropyl-β-thiogalactopyranoside induction. The protein was purified by affinity chromatography in a HisTrap HP column (GE Healthcare, Waukesha, WI). Detailed procedures are in the Supplementary information.

Enzyme-linked immunosorbent assay (ELISA). TGF-β2 ELISA was performed using a TGF-β2 Emax® Immune Assay System ELISA kit (Promega, Madison, WI) according to the manufacturer's instructions.

Luciferase assay. The mink lung epithelial cell line CCL64, which stably expressed $(CAGA)_9$-MLP-luciferase and contained nine copies of a Smad-binding CAGA box element upstream of a minimal adenovirus major late promoter (2×10^4 cells/well)[23], was seeded into 96-well plates. The next day, the medium was replaced with fresh medium containing 0.1% bovine serum albumin, and the cells were cultured for an additional 24 hours. The cells were extracted with lysis buffer, and luciferase activity was measured by a Luciferase Assay System (Promega, Madison, WI) according to the manufacturer's instructions.

Real-time RT-PCR. The isolation of total RNA and real-time RT-PCR were performed as described previously[24]. Briefly, total RNA was extracted using the RNeasy mini kit (Qiagen, Valencia, CA) according to the manufacturer's protocols. RNA (0.5 μg) was reverse transcribed to cDNA using the PrimeScript® RT Master Mix (Takara Bio Inc., Shiga, Japan). The mRNA expression levels were determined using real-time PCR. Real-time PCR was performed with the Thermal Cycler Dice® Real Time System, using the SsoAdvanced™ SYBR® Green Supermix (Bio-Rad Laboratories, Hercules, CA) and normalized to GAPDH mRNA expression. The primer sequences used were as follows: human TGF-β1 forward: 5′-ACT ATT GCT TCA GCT CCA CGG A-3′, reverse: 5′-GGT CCT TGC GGA AGT CAA TGT A-3′; human collagen α1 (I) forward: 5′-ACG AAG ACA TCC CAC CAA TC-3′, reverse: 5′-AGA TCA CGT CAT CGC ACA AC-3′; human GAPDH forward: 5′-GGA GTC AAC GGA TTT GGT-3′, reverse: 5′-AAG ATG GTG ATG GGA TTT CCA-3′; and human TβRI forward: 5′-CTT AAT TCC TCG AGA TAG GC-3′, reverse: 5′-GTG AGA TGC AGA CGA AGC-3′.

Immunofluorescence staining. The cells were grown on eight-well chamber slides or glass bottom dishes and were incubated with HCV virion for 24 hours at 37°C. The cells were washed with PBS, fixed with 4% paraformaldehyde for 10 min at room temperature, and permeabilized with 0.1% Triton X-100 for 20 min at room temperature. After blocking with 3% BSA/10% normal goat serum/PBS for 30 min, the cells were incubated with primary antibodies for 2 hours, followed by incubation with secondary antibodies for 30 min at RT. For detecting NS3 and TβRI on the cell surface, the cells were fixed without permeabilization after incubation with the secondary antibodies. After being washed with PBS, the cells were mounted with Vectashield DAPI mounting medium (Vector Laboratories, Inc., Burlingame, CA) and observed under a Zeiss LSM 700 laser scanning confocal microscope. For quantitative fluorescence analyses, the intensity of phosphorylated Smad3 and the colocalization of NS3 and TβRI (Pearson's colocalization coefficient values) in each panel were calculated with ZEN software.

Proximity ligation assay (PLA). HCV-infected Huh-7.5.1 cells were fixed with 4% paraformaldehyde for 10 min at room temperature and subjected to in situ PLA using a Duolink in situ red starter kit (Olink Bioscience, Uppsala, Sweden) according to the manufacturer's instructions. Briefly, cells were blocked and incubated with primary antibodies against NS3 and TβRI, followed by incubation with the PLA probes, which were secondary antibodies (anti-mouse and anti-rabbit) conjugated to oligonucleotides. DNA ligase was added to enable the formation of circular DNA strands when the PLA probes were in close proximity. This step was followed by incubation with oligonucleotides and polymerase for rolling circle amplification[25]. Texas red-labeled oligonucleotides, which hybridize to the amplified products, were used for visualization. The cells were observed under a Zeiss LSM 700 laser scanning confocal microscope.

Immunoprecipitation and immunoblotting. Anti-FLAG M2 affinity beads were pretreated with 5% bovine serum albumin in 20 mM Tris-HCl, pH 7.5, 150 mM NaCl overnight. Isotype control IgG was bound to Protein G PLUS-Agarose (Santa Cruz) pretreated with 5% bovine serum albumin in 20 mM Tris-HCl, pH 7.5, 150 mM NaCl. Cell lysates with 3xFLAG or 3x-FLAG-NS3 (2 mg protein) were incubated with 50 μl of the beads (10% slurry) at 4°C for 3 hours. The beads were then washed three times with the lysis buffer and incubated with lysates containing 6xHis-TβRI or 6xHis-TβRII (0.5 mg protein) at 4°C overnight. The bound proteins were eluted with the SDS-PAGE sample buffer after washing four times with the lysis buffer and then were subjected to SDS-PAGE (15% acrylamide) followed by transfer onto a PVDF membrane (Pall). The proteins were then visualized using anti-His tag HRP DirectT (MBL, 1/5000) or anti-FLAG BioM2 antibody (Sigma, 10 μg/ml) and horseradish peroxidase-conjugated anti-biotin antibody (Cell Signaling) using the ECL Western blotting detection reagent (GE Healthcare).

In silico docking simulation. The protein-protein docking simulation was implemented based on the geometric complementarity[26] between NS3 protease (PDB ID, 1NS3) and TβRI (PDB ID, 2PJY). Specifically, coordinates of the proteins were projected onto three-dimensional grids separated from each other at regular intervals. A surface score and an intramolecular score were assigned to each grid. This operation was conducted for both the receptor and the ligand. Next, convolution between the obtained grids was performed, the surfaces were explored exhaustively, and the complementarities of the binding states were calculated based on the scores. Amino acid residues appearing frequently in binding states with high complementarity scores can be estimated to be residues that are highly likely to appear in the interaction with an actual receptor. Accordingly, amino acid residues with an interatomic distance of 3.8 Å or less in the putative binding states were defined as contact residues and regarded as the putative contact residues of NS3 and TβRI.

Animal experiment. Chimeric mice with humanized livers were generated as previously described using urokinase-type plasminogen activator (uPA)-transgenic/SCID mice[27]. All mice were transplanted with frozen human hepatocytes obtained from a single donor. All animal experiments were approved by RIKEN Institutional Animal Use and Care Administrative Advisory Committees and were performed in accordance with RIKEN guidelines and regulations. Infection, extraction of serum samples, and euthanasia were performed under isoflurane anesthesia. Male chimeric mice (12- to 14-week old) were intravenously injected with 100 μl HCV J6/JFH-1 strain (1×10^8 copies/ml). Four weeks after HCV inoculation, anti-NS3 antibodies against predicted binding sites with the TβRI receptor were administered at doses of 0.5 mg/kg of BW or 5 mg/kg of BW twice a week for twelve weeks. Normal mouse IgG was administered at a dose of 5 mg/kg of BW as a control. When the animals were euthanized, the livers were either fixed with 4% paraformaldehyde for histological analysis or frozen immediately in liquid nitrogen for mRNA isolation.

Staining of liver tissue sections. The liver tissues were fixed in 4% paraformaldehyde and embedded in paraffin, and tissue sections (6 μm in thickness) were prepared with a Leica sliding microtome (Leica Microsystems, Nussloch, Germany). The liver tissue sections were deparaffinized, rehydrated, and incubated for 5 min with a drop of Proteinase K (Dako Envision) in 2 mL of 0.05 M Tris-HCl buffer (pH 7.5) at room temperature. The liver tissue sections were stained with Mayer's hematoxylin solution (Muto Chemicals) and 1% eosin Y solution (Muto Chemicals). Sirius Red, which results in a red staining of all fibrillar collagen, was used to evaluate fibrosis. Briefly, the liver sections were stained with 0.05% Fast Green FCF (ChemBlink, Inc. CAS: 2353-45-9) and 0.05% Direct Red 80 (Polysciences, Inc. CAS: 2610-10-18) in saturated picric acid (Muto Chemicals) for 90 min at room temperature. The ratios of Sirius Red positive/total area (%) from 6 randomly selected fields were measured for each group using WinROOF software (Mitani Corp., Tokyo, Japan).

Statistics. Statistical analysis was performed using one-way analysis of variance, followed by Dunnett's post-hoc test. A two-tailed Student's *t*-test was used to evaluate differences between the two groups. The Kruskal-Wallis test followed by Dunn's post-hoc test was used for multiple comparisons of Sirius Red positive areas.

1. Marazzi, I. *et al.* Suppression of the antiviral response by an influenza histone mimic. *Nature* **120**, 428–433 (2012).
2. Chaurushiya, M. S. *et al.* Viral E3 ubiquitin ligase-mediated degradation of a cellular E3: viral mimicry of a cellular phosphorylation mark targets the RNF8 FHA domain. *Mol. Cell.* **123**, 352–364 (2012).
3. Tong, M. J., el-Farra, N. S., Reikes, A. R. & Co, R. L. Clinical outcomes after transfusion-associated hepatitis C. *N. Engl. J. Med.* **332**, 1463–1466 (1995).
4. Poynard, T., Yuen, M. F., Ratziu, V. & Lai, C. L. Viral hepatitis C. *Lancet* **362**, 2095–2100 (2003).
5. Lavanchy, D. Chronic viral hepatitis as a public health issue in the world. *Best Pract Res Clin. Gastroenterol.* **22**, 991–1008 (2008).
6. Moradpour, D., Penin, F. & Rice, C. M. Replication of hepatitis C virus. *Nat. Rev. Microbiol.* **5**, 453–463 (2007).
7. Raney, K. D., Sharma, S. D., Moustafa, I. M. & Cameron, C. E. Hepatitis C virus non-structural protein 3 (HCV NS3): a multifunctional antiviral target. *J. Biol. Chem.* **285**, 22725–22731 (2010).
8. Okuno, M. *et al.* Prevention of rat fibrosis by protease inhibitor, Camostat Mesilate, via reduced generation of active TGF-β. *Gastroenterology* **120**, 1784–1800 (2001).
9. Akita, K. *et al.* Impaired liver regeneration in mice by lipopolysaccharide via TNF-α/kallikrein-mediated activation of latent TGF-β. *Gastroenterology* **123**, 352–364 (2002).
10. Ikushima, H. & Miyazono, K. TGFβ signalling: a complex web in cancer progression. *Nat. Rev. Cancer* **10**, 415–424 (2010).
11. Taniguchi, H. *et al.* Hepatitis C virus core protein upregulates transforming growth factor-β1 transcription. *J. Med. Virol.* **72**, 52–59 (2004).
12. Coenen, M. *et al.* Hepatitis C virus core protein induces fibrogenic actions of hepatic stellate cells via toll-like receptor 2. *Lab. Invest.* **91**, 1375–1382 (2011).
13. Wu, C. F., Lin, Y. L. & Huang, Y. T. Hepatitis C virus core protein stimulates fibrogenesis in hepatic stellate cells involving the obese receptor. *J. Cell. Biochem.* **114**, 541–550 (2012).
14. Presser, L. D., Haskett, A. & Waris, G. Hepatitis C virus-induced furin and thrombospondin-1 activate TGF-β1: Role of TGF-β1 in HCV replication. *Virology* **412**, 286–296 (2011).

15. Romano, K. P. *et al.* Molecular mechanisms of viral and host cell substrate recognition by hepatitis C virus NS3/4A protease. *J. Virol.* **85**, 6106–6116 (2011).
16. Kwong, A. D., Kauffman, R. S., Hurter, P. & Mueller, P. Discovery and development of telaprevir: an NS3-4A protease inhibitor for treating genotype 1 chronic hepatitis C virus. *Nat. Biotechnol.* **29**, 993–1003 (2011).
17. Toyoda, M. *et al.* Role of serum soluble Fas/soluble Fas ligand and TNF-α on response to interferon-α therapy in chronic hepatitis C. *Liver* **20**, 305–311 (2000).
18. Lecube, A., Hernandez, C., Genesca, J. & Simo, R. Proinflammatory cytokines, insulin resistance, and insulin secretion in chronic hepatitis C patients: A case-control study. *Diabetes Care* **29**, 1096–1101 (2006).
19. Chouteau, P. *et al.* Hepatitis C virus (HCV) protein expression enhances hepatic fibrosis in HCV transgenic mice exposed to a fibrogenic agent. *J. Hepatol.* **57**, 499–507 (2012).
20. Muller, D. A. & Young, P. R. The flavivirus NS1 protein: Molecular and structural biology, immunology, role in pathogenesis and application as a diagnostic biomarker. *Antiviral Res.* **98**, 192–208 (2013).
21. Zhang, Z. X., Sonnerborg, A. & Sallberg, M. A cell-binding Arg-Gly-Asp sequence is present in close proximity to the major linear antigenic region of HCV NS3. *Biochem. Biophys. Res. Commun.* **202**, 1352–1356 (1994).
22. Alcon, S. *et al.* Enzyme-linked immunosorbent assay specific to Dengue virus type 1 nonstructural protein NS1 reveals circulation of the antigen in the blood during the acute phase of disease in patients experiencing primary or secondary infections. *J. Clin. Microbiol.* **40**, 376–81 (2002).
23. Datta, P. K. & Moses, H. L. STRAP and Smad7 synergize in the inhibition of transforming growth factor beta signaling. *Mol. Cell. Biol.* **20**, 3157–3167 (2000).
24. Tatsukawa, H. *et al.* Role of transglutaminase 2 in liver injury via cross-linking and silencing of transcription factor Sp1. *Gastroenterology* **136**, 1783–1795 (2009).
25. Soderberg, O. *et al.* Characterizing proteins and their interactions in cells and tissues using the *in situ* proximity ligation assay. *Methods* **45**, 227–232 (2008).
26. Katchalski-Katzir, E. *et al.* Molecular surface recognition: determination of geometric fit between proteins and their ligands by correlation techniques. *Proc. Natl. Acad. Sci. USA* **89**, 2195–2199 (1992).
27. Tateno, C. *et al.* Near completely humanized liver in mice shows human-type metabolic responses to drugs. *Am. J. Pathol.* **165**, 901–912 (2004).

Acknowledgments

We are indebted to Mr. Kazushige Katsura and Ms. Chiemi Mishima-Tsumagari (RIKEN Systems and Structural Biology Center, Kanagawa, Japan; Division of Structural and Synthetic Biology, RIKEN Center for Life Science Technologies, Yokohama, Japan) for preparing and providing recombinant NS3, and Dr. Takashi Shimada, Dr. Chise Tateno, and Dr. Masakazu Kakuni (PhenixBio Co., Ltd., Hiroshima, Japan) for helpful discussions regarding the animal experiment. This work was supported in part by a Grant-in-Aid for Scientific Research from the Ministry of Education, Culture, Sports, Science and Technology (23390202 to S.K.), and Grants for Collaborative Researchers from Industries (to K.S.), Program for Drug Discovery and Medical Technology Platforms (to S.K.), and Chemical Genomics Research Program (to S.K.) from RIKEN.

Author contributions

Sakata K., Hara M. and Yaguchi S. performed experiments. Sakata K., Matsuura T., Miyazawa K., Imoto M. and Kojima S. wrote the manuscript. Terada T., Matsumoto T., Shirouzu M., Yokoyama S., Yamaguchi T. and Suzuki T. contributed to the production and the purification of recombinant NS3 and its antibodies. Watanabe N., Aizaki H. and Wakita T. contributed to the production and the purification of HCV and discussion from the point of view of virology. Takaya D. performed docking simulation to predict binding sites. Sakata K. and Kojima S. planned the research. Kojima S. supervised the entire project.

Additional information

Supplementary information accompanies this paper at http://www.nature.com/scientificreports

Competing financial interests: The authors declare no competing financial interests.

How to cite this article: Sakata, K. *et al.* HCV NS3 protease enhances liver fibrosis via binding to and activating TGF-β type I receptor. *Sci. Rep.* **3**, 3243; DOI:10.1038/srep03243 (2013).

OPEN ACCESS Freely available online

PLOS ONE

The Effect of Acyclic Retinoid on the Metabolomic Profiles of Hepatocytes and Hepatocellular Carcinoma Cells

Xian-Yang Qin[1,5], Feifei Wei[2,5], Masaru Tanokura[2], Naoto Ishibashi[3], Masahito Shimizu[4], Hisataka Moriwaki[4], Soichi Kojima[1]*

1 Micro-signaling Regulation Technology Unit, RIKEN Center for Life Science Technologies, Wako, Saitama, Japan, **2** Department of Applied Biological Chemistry, Graduate School of Agricultural and Life Sciences, University of Tokyo, Tokyo, Japan, **3** Tokyo New Drug Research Laboratories, Pharmaceutical Division, KOWA Company, Ltd., Tokyo, Japan, **4** Department of Gastroenterology, Gifu University Graduate School of Medicine, Gifu, Japan, **5** Japan Society for the Promotion of Science, Tokyo, Japan

Abstract

Background/Purpose: Acyclic retinoid (ACR) is a promising chemopreventive agent for hepatocellular carcinoma (HCC) that selectively inhibits the growth of HCC cells (JHH7) but not normal hepatic cells (Hc). To better understand the molecular basis of the selective anti-cancer effect of ACR, we performed nuclear magnetic resonance (NMR)-based and capillary electrophoresis time-of-flight mass spectrometry (CE-TOFMS)-based metabolome analyses in JHH7 and Hc cells after treatment with ACR.

Methodology/Principal Findings: NMR-based metabolomics revealed a distinct metabolomic profile of JHH7 cells at 18 h after ACR treatment but not at 4 h after ACR treatment. CE-TOFMS analysis identified 88 principal metabolites in JHH7 and Hc cells after 24 h of treatment with ethanol (EtOH) or ACR. The abundance of 71 of these metabolites was significantly different between EtOH-treated control JHH7 and Hc cells, and 49 of these metabolites were significantly down-regulated in the ACR-treated JHH7 cells compared to the EtOH-treated JHH7 cells. Of particular interest, the increase in adenosine-5′-triphosphate (ATP), the main cellular energy source, that was observed in the EtOH-treated control JHH7 cells was almost completely suppressed in the ACR-treated JHH7 cells; treatment with ACR restored ATP to the basal levels observed in both EtOH-control and ACR-treated Hc cells (0.72-fold compared to the EtOH control-treated JHH7 cells). Moreover, real-time PCR analyses revealed that ACR significantly increased the expression of pyruvate dehydrogenase kinases 4 (PDK4), a key regulator of ATP production, in JHH7 cells but not in Hc cells (3.06-fold and 1.20-fold compared to the EtOH control, respectively).

Conclusions/Significance: The results of the present study suggest that ACR may suppress the enhanced energy metabolism of JHH7 cells but not Hc cells; this occurs at least in part via the cancer-selective enhancement of PDK4 expression. The cancer-selective metabolic pathways identified in this study will be important targets of the anti-cancer activity of ACR.

Citation: Qin X-Y, Wei F, Tanokura M, Ishibashi N, Shimizu M, et al. (2013) The Effect of Acyclic Retinoid on the Metabolomic Profiles of Hepatocytes and Hepatocellular Carcinoma Cells. PLoS ONE 8(12): e82860. doi:10.1371/journal.pone.0082860

Editor: Matias A. Avila, University of Navarra School of Medicine and Center for Applied Medical Research (CIMA), Spain

Received August 11, 2013; **Accepted** November 6, 2013; **Published** December 23, 2013

Funding: This study was supported by the Japan Society for the Promotion of Science (JSPS) Postdoctoral Fellowship for Foreign Researchers. This study was also partly supported by the HMT Research Grant for Young Leaders in Metabolomics 2012 from Human Metabolome Technologies Inc. The funders had no role in the study design, data collection and analysis, decision to publish, or preparation of the manuscript.

Competing Interests: Co-author Naoto Ishibashi is employed by KOWA Company Ltd. This study was partly supported by the HMT Research Grant for Young Leaders in Metabolomics 2012 from Human Metabolome Technologies Inc. There are no patents, products in development or marketed products to declare. This does not alter the authors' adherence to all the PLOS ONE policies on sharing data and materials.

* E-mail: skojima@postman.riken.go.jp

Introduction

Hepatocellular carcinoma (HCC) represents approximately 85% of all primary liver cancers and is one of the most common malignancies worldwide, especially in Eastern Asia [1]. The prognosis of HCC remains very poor; this poor prognosis is due in part to its high rate of recurrence after initial treatment, which reaches approximately 70% within 5 years [2]. Acyclic retinoid (ACR), a synthetic retinoid with a vitamin A-like structure, prevents the recurrence and development of HCC in patients after the surgical removal of primary tumors [3,4]. ACR is currently undergoing phase II/III clinical trials (JapicCTI-121828) in Japan and is expected to become the first chemopreventive agent.

Another important characteristic of ACR is that it selectively suppresses the growth of HCC cells (JHH7 and others) but not normal hepatic cells (Hc) [5,6]. Although the mechanism underlying this effect is not fully understood, previous basic and clinical studies by our group and others have suggested that both non-genomic and genomic signaling pathways may be responsible for the cancer-selectivity of ACR [5,7,8,9,10,11,12]. A typical example is the prevention by ACR of the aberrant hyper-phosphorylation and inactivation of retinoid X receptor (RXR) α

that occurs during carcinogenesis in HCC [12] and the subsequent induction of apoptosis in HCC cells by the restoration of the expression of RXRα downstream genes such as p21 [11], transglutaminase 2 (TG2) [5] and more. However, to the best of our knowledge, no information is available regarding the effect of ACR on the metabolism of HCC cells.

Recently, the approach of targeting cancer metabolism to develop and improve cancer therapeutics has received a great deal of attention [13]. A distinguishing feature of cancer is that the metabolic pathways of cancer cells are adapted to support rapid and uncontrolled cell proliferation. One of the best-known alterations in cancer cell metabolism is a switch from mitochondrial oxidative phosphorylation to cytoplasmic glycolysis; this switch is known as the Warburg effect [14]. It is possible that targeting cellular metabolism may suppress cancer. In fact, several metabolism-targeting therapies have been already proven to be effective in the treatment of diverse human tumors [13,15].

Although chronic hepatitis B virus (HBV) or hepatitis C virus (HCV) infections are believed to account for approximately 80% of HCC [16], a growing body of evidence indicates that metabolic syndrome is also a risk factor for the development of HCC [17]. Indeed, it is extremely difficult to find a single essential target for cancer therapeutics, due to the remarkable heterogeneity and adaptability of cancer cells. It is likely that further investigations into the effect of ACR on cancer cell metabolism will improve our understanding of the molecular pathways underlying the cancer-selective growth suppressive effect of ACR and benefit the development of more effective cancer drugs and therapies against HCC. To achieve this, both nuclear magnetic resonance (NMR)-based and capillary electrophoresis time-of-flight mass spectrometry (CE-TOFMS)-based metabolome analyses were performed in JHH7 and Hc cells after treatment with ACR.

Materials and Methods

Materials

ACR (NIK-333) was supplied by Kowa Co. Ltd. (Tokyo, Japan). All-*trans*-retinoic acid (AtRA) was purchased from Sigma-Aldrich (St Louis, MO, USA). Ethanol (EtOH) was obtained from Wako Industries (Osaka, Japan), and used as the primary solvent for all reagents. EtOH solutions were further diluted into cell culture media for treatments. The final concentration of EtOH in media used as a control was 0.05% (vol/vol).

Cell culture

The JHH7 HCC cell line was kindly supplied by Dr. Matsuura (Jikei University School of Medicine, Tokyo, Japan) [18]. The normal human hepatocyte cell line (Hc) was purchased from Cell Systems (Kirkland, WA, USA). Both cell lines were maintained in Dulbecco's Modified Eagle Medium (DMEM; Wako Industries) containing 10% fetal bovine serum (FBS, Mediatech, Herndon, VA, USA), 100 U/ml penicillin/streptomycin and 2 mmol/L L-glutamine (Mediatech, Herndon, VA, USA) and grown at 37°C in a humidified 5% CO_2 incubator. For chemical treatment, the cells were cultured in serum-free media containing EtOH or ACR at the appropriate concentrations.

NMR-based metabolomics

For NMR analyses, cells (approximately 1×10^7 cells) treated with EtOH control or 10 μM ACR control for 4 h or 18 h were harvested by scraping as previously described [19]. The one-dimensional (1D) ^{1}H spectra were measured at 500 MHz on a Varian Unity INOVA-500 spectrometer. All NMR spectra were processed using the MestReNova program (Version 5.3.0, MestRec, Santiago de Compostela, Spain). Metabolites were identified using publicly accessible databases, including BioMagRes data bank (http://www.bmrb.wisc.edu), the Metabolomics Database of Linkoping (http://www.mdl.imv.liu.se), and the Human Metabolome Data Bank (http://www.hmdb.ca). Detailed NMR methods have been described previously [19,20].

CE-TOFMS analyses

JHH7 and Hc cells (approximately 5×10^6 cells) treated with EtOH control or 10 μM ACR for 24 h were washed twice with a 5% mannitol solution, and then 1,300 μL of a methanol solution containing 10 μM internal standards was added. Metabolome extraction was then performed as previously described [21]. The metabolic profiles of the cells were then measured using a CE-TOFMS-based metabolomics technique, which is a novel strategy for analyzing and differentially displaying metabolic profiles [21]. CE-TOFMS was carried out using an Agilent CE Capillary Electrophoresis System equipped with an Agilent 6210 Time-of-Flight mass spectrometer, Agilent 1100 isocratic HPLC pump, Agilent G1603A CE-MS adapter kit, and Agilent G1607A CE-ESI-MS sprayer kit (Agilent Technologies, Waldbronn, Germany).

Data analysis for CE-TOFMS and metabolite identification

The raw data obtained by CE-TOFMS were analyzed using KEIO MasterHands software exactly as previously described [22,23]. Briefly, the injected volume for CE and the sensitivity of MS were corrected using internal standards, and then all the annotated metabolites were further corrected to the same chemicals in a standard mixture to overcome different ionization patterns. The peaks were identified based on the matched mass-to-charge ratio (m/z) values and normalized migration times of the corresponding standard compounds.

Real-time RT-PCR

For PCR analyses, RNA was isolated from each cell culture treated with EtOH, AtRA or ACR for 4 h using an RNeasy Kit (Qiagen, Valencia, CA, USA), and the amount and purity of the isolated RNA were evaluated using a NanoDrop spectrophotometer (NanoDrop products, Wilmington, DE, USA). cDNA was then synthesized using a PrimeScript RT Master Mix Kit (TaKaRa Bio, Otsu, Japan). Oligonucleotide primers were designed using OligoPerfect Designer software (Invitrogen, Carlsbad, CA, USA; http://www.tools.invitrogen.com) and synthesized by Invitrogen. The sequences of the primers and the full gene names are summarized in Table S1. PCR reactions were performed using a the Thermal Cycler Dice™ Real Time System (TP8000; Takara Bio) with SsoAdvanced™ SYBR® Green Supermix (Bio-Rad Laboratories, Hercules, CA, USA).

Western blot analysis

JHH7 and Hc cells treated with EtOH, AtRA and ACR for 24 h were lysed using RIPA buffer. After boiling at 97°C for 10 min, the protein samples were resolved by sample buffer for sodium dodecyl sulfate (SDS) polyacrylamide gel electrophoresis, run on a 10% gel and transferred to a polyvinylidene difluoride membrane (Bio-Rad Laboratories). The membranes were blocked with 5% nonfat dry milk in Tris-buffered saline (TBS) and 0.1% Tween and then probed with primary antibodies against pyruvate dehydrogenase kinase 4 (PDK4; sc-14492; 1:1,000 dilution, Santa Cruz Biotechnology, CA, USA), pyruvate dehydrogenase (lipoamide) alpha 1 (PDHA1; sc-377092; 1:1,000 dilution, Santa Cruz Biotechnology), phospho-PDHA1 (ab92696; 1:1,000 dilution, Abcam) or Lamin B1 (ab16048; 1:5,000 dilution, Santa Cruz

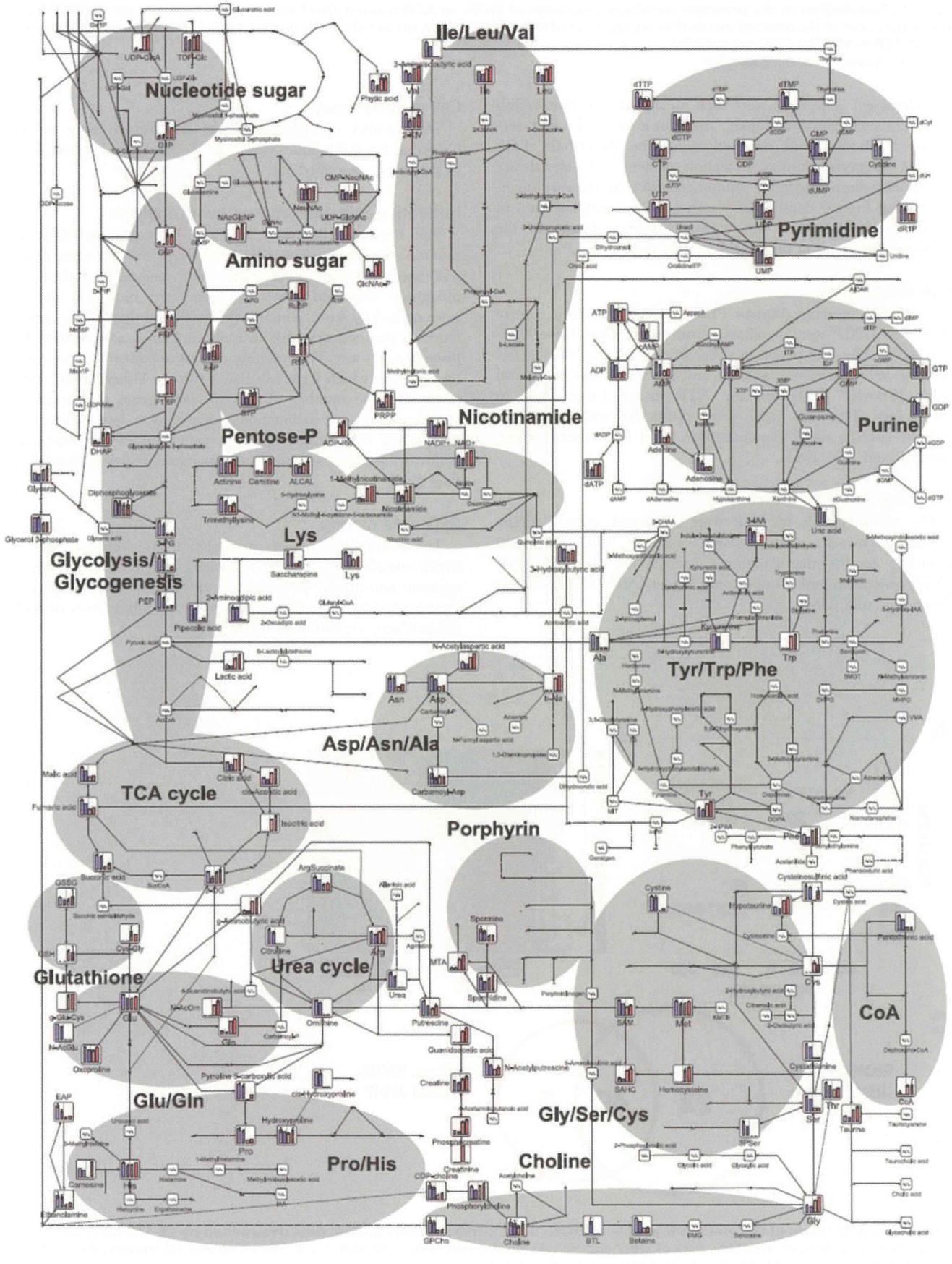
Nucleotide sugar
Ile/Leu/Val
Amino sugar
Pyrimidine
Nicotinamide
Pentose-P
Purine
Lys
Glycolysis/
Glycogenesis
Tyr/Trp/Phe
Asp/Asn/Ala
TCA cycle
Porphyrin
Urea cycle
Glutathione
CoA
Glu/Gln
Gly/Ser/Cys
Pro/His
Choline

Figure 1. Metabolites in the principle metabolic pathways of EtOH- or ACR-treated JHH7 and Hc cells detected by CE-TOFMS. The relative quantities of the detected metabolites are represented as bar graphs (from left to right: EtOH-treated JHH7, ACR-treated JHH7, EtOH-treated Hc, and ACR-treated Hc). N.D., not detected.
doi:10.1371/journal.pone.0082860.g001

Biotechnology). The blots were then incubated with horseradish peroxidase-conjugated anti-goat, anti-mouse or anti-rabbit secondary antibodies and detected using the Amersham ECL PlusTM Western Blotting Detection System (GE Healthcare UK, Buckingham, England). Immunoreactive bands were quantified using ImageJ densitometry software (National Institutes of Health, Bethesda, MD), and normalized; the density of the corresponding band in the EtOH control was set to 1.0.

RNA interference

An siRNA targeting human PDK4 (sc-39030) and a control siRNA (sc-37007) were purchased from Santa Cruz Biotechnology. JHH7 cells were plated in either 96-well plates (1×10^4 cells/well) for cell proliferation analysis and RNA isolation or 60-mm dishes (3.5×10^5 cells/dish) for ATP assays 1 day prior to transfection. The cells were then transfected with 50 nM or 100 nM siRNAs using Lipofectamine 2000 (Life Technologies, Grand Island, NY, USA).

ATP assay

The cellular levels of ATP were measured using a firefly bioluminescence assay kit (AMERIC-ATP kit, Wako Industries) according to the manufacturer's instructions. The luciferase activity was measured using a plate reader (ARVO MX, Perkin Elmer Inc., MA, USA).

Cell viability assay

The number of viable cells was determined using the Cell Counting Kit-8 (Dojindo Molecular Technologies, Tokyo, Japan) as previously described [5].

Network generation and pathway analyses

The Ingenuity Pathways Analysis (IPA) program (Ingenuity Systems, Mountain View, CA, USA; http://www.ingenuity.com) was used to identify networks and canonical pathways as previously described [24]. The generated biological networks were ranked by score, which is the likelihood that a set of genes is found in the networks due to random chance as measured by a Fisher's exact test. The resulting canonical pathways were ranked by *P* values, which were calculated using a Fisher's exact test by comparing the number of user-specified genes of interest that participate in a given function or pathway, relative to the total number of occurrences of these genes in all the functional/pathway annotations stored in the Ingenuity Pathways Knowledge Base [25].

GEO data mining

The normalized PDK4 expression from a clinical data set, which contains transcriptome profiling of 268 HCC tumor, 243 adjacent non-tumor, 40 cirrhotic and 6 healthy liver samples, was downloaded from the Gene Expression Omnibus (www.ncbi.nlm.nih.gov/geo, accession no. GSE25097).

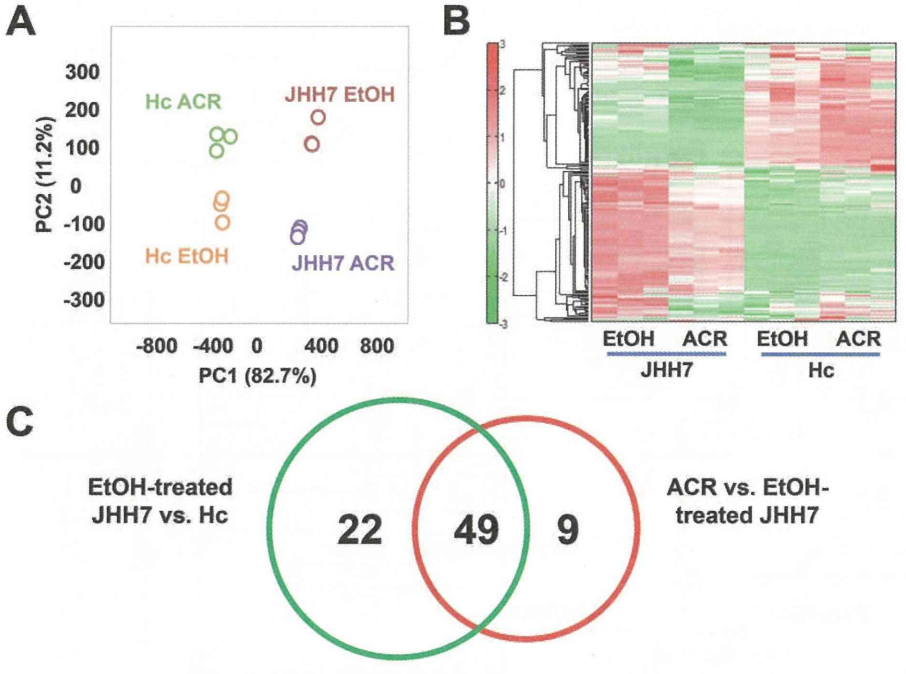

Figure 2. A comparison of the metabolic profile of EtOH- or ACR-treated JHH7 and Hc cells determined by CE-TOFMS. PCA scoreplot (*A*) and heat map (*B*) from metabolic data of JHH7 and Hc cells treated with EtOH and ACR ($n=3$). Venn-diagrams (*C*) showing the number of metabolites that were significantly deregulated between the two groups.
doi:10.1371/journal.pone.0082860.g002

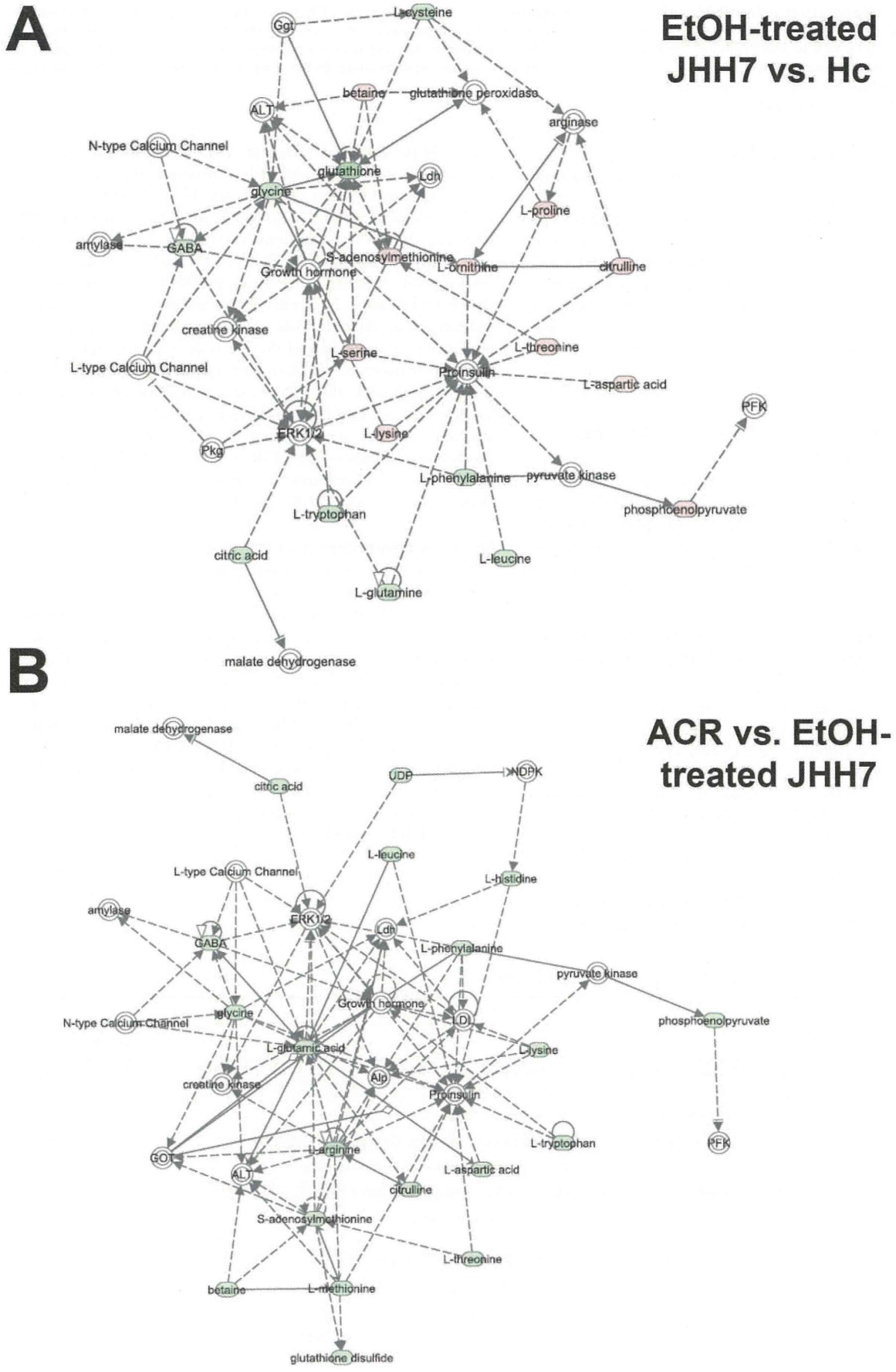
A
EtOH-treated JHH7 vs. Hc
Ggt
L-cysteine
betaine
glutathione peroxidase
ALT
arginase
N-type Calcium Channel
glutathione
Ldh
glycine
L-proline
amylase
GABA
S-adenosylmethionine
L-ornithine
citrulline
Growth hormone
creatine kinase
L-threonine
L-serine
L-type Calcium Channel
Proinsulin
L-aspartic acid
PFK
ERK1/2
L-lysine
Pkg
L-phenylalanine
pyruvate kinase
L-tryptophan
phosphoenolpyruvate
citric acid
L-leucine
L-glutamine
malate dehydrogenase
B
ACR vs. EtOH-treated JHH7
malate dehydrogenase
citric acid
UDP
NDPK
L-leucine
L-type Calcium Channel
L-histidine
amylase
ERK1/2
Ldh
GABA
L-phenylalanine
pyruvate kinase
Growth hormone
glycine
LDL
N-type Calcium Channel
phosphoenolpyruvate
L-glutamic acid
L-lysine
creatine kinase
Alp
Proinsulin
L-tryptophan
PFK
GOT
L-arginine
ALT
L-aspartic acid
citrulline
S-adenosylmethionine
L-threonine
betaine
L-methionine
glutathione disulfide